

Dephosphorylation of D-Peptide Derivatives to Form Biofunctional, Supramolecular Nanofibers/Hydrogels and Their Potential Applications for Intracellular Imaging and Intratumoral Chemotherapy

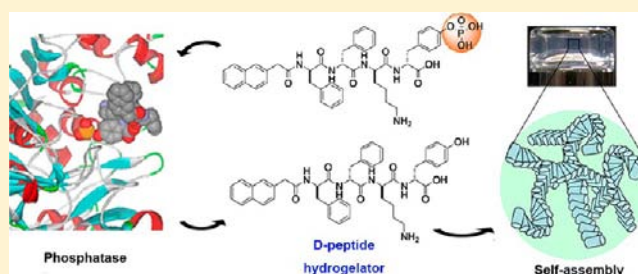
Jiayang Li,[†] Yuan Gao,[†] Yi Kuang,[†] Junfeng Shi,[†] Xuewen Du,[†] Jie Zhou,[†] Huaimin Wang,[‡] Zhimou Yang,[‡] and Bing Xu^{*,†}

[†]Department of Chemistry, Brandeis University, 415 South Street, Waltham, Massachusetts 02454, United States

[‡]State Key Laboratory of Medicinal Chemical Biology and College of Life Sciences, Nankai University, Tianjin 300071, People's Republic of China

S Supporting Information

ABSTRACT: D-Peptides, as the enantiomers of the naturally occurring L-peptides, usually resist endogenous proteases and are presumably insensitive to most enzymes. But, it is unclear whether or how a phosphatase catalyzes the dephosphorylation from D-peptides. In this work, we examine the formation of the nanofibers of D-peptides via enzymatic dephosphorylation. By comparing the enzymatic hydrogelation of L-peptide and D-peptide based hydrogelators, we find that the chirality of the precursors of the hydrogelators affects little on the enzymatic hydrogelation resulted from the removal of the phosphate group from a tyrosine phosphate residue. The attachment of a therapeutic agent (e.g., taxol) or a fluorophore (e.g., 4-nitro-2,1,3-benzoxadiazole) to the D-peptide based hydrogelators affords a new type of biostable or biocompatible hydrogelators, which may find applications in intratumoral chemotherapy or intracellular imaging, respectively. This work, as the first comprehensive and systematic study of the unexpected enzymatic dephosphorylation of D-peptides, illustrates a useful approach to generate supramolecular hydrogels that have both biostability and other desired functions.



INTRODUCTION

This study investigates the use of alkaline phosphatase to generate supramolecular hydrogels of D-peptide derivatives and explores the potential applications of this apparently anti-intuitive enzyme-instructed self-assembly process. As the result of the self-assembly of certain small molecules (i.e., hydrogelators^{1–4}) in water, supramolecular nanofibers act as entangled matrices for holding large amounts of water and result in hydrogels that are referred to as supramolecular hydrogels.² Largely because of their inherent biocompatibility and biodegradability originated from the supramolecular (i.e., noncovalent) nature of the nanofibers formed by molecular self-assembly, supramolecular hydrogels are emerging as a relatively new class of biomaterials and are finding increased applications in biomedicine, such as tissue engineering,⁵ drug delivery,^{3,6} biosensing,^{7,8} wound healing,⁹ enzyme assays,¹⁰ gel electrophoresis,¹¹ nucleic acid sequestration,¹² and protein separation.¹³ Among a variety of molecules that serve as hydrogelators, small peptide-based hydrogelators¹⁴ have attracted considerable attention because of the well-established synthesis procedure (e.g., SPPS)¹⁵ and the obvious biological relevance of peptides. Most of the peptide-based hydrogelators, being made of L-amino acids (i.e., L-peptides), not only preserve

the biological functions of a peptide motif but also serve as the native substrates of enzymes.

As an alternative process of the use of enzymes to cross-link polymers to cause rapid hydrogelation,¹⁶ small peptides made of L-amino acid residues undergo a process referred to as enzymatic hydrogelation that the solution of a precursor of a hydrogelator, upon the addition of an enzyme, turns into the gel of the corresponding hydrogelator.¹⁷ As a useful strategy for generating supramolecular nanofibers/hydrogels, enzymatic hydrogelation has already found a wide range of applications, such as screening the inhibitors of enzymes,¹⁸ measuring enzyme activity,⁸ modulating biomineralization,¹⁹ typing bacteria,²⁰ delivering drugs or proteins,^{21,22} stabilizing enzymes,²³ and regulating the fate of cells.²⁴ Despite the merits of L-peptides as the substrates for enzymatic hydrogelation, L-peptides are susceptible to degradation catalyzed by various endogenous proteases, which limits the applications of supramolecular hydrogels when long-term biostability are required (such as controlled drug release,^{6,25} intracellular imaging,²⁶ or other in vivo applications). Therefore, it is

Received: April 28, 2013

Published: June 6, 2013

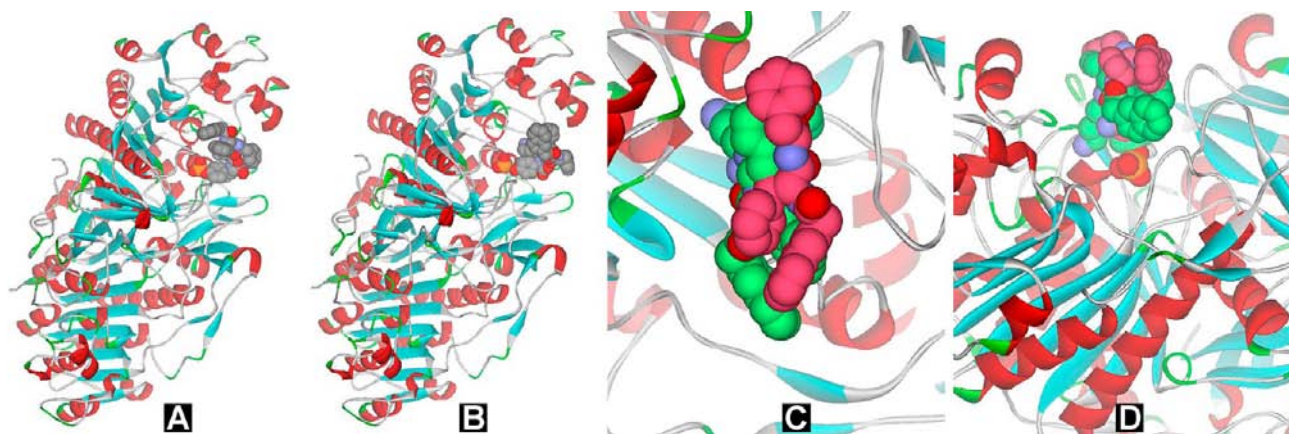


Figure 1. Binding of the phosphate precursors (presented as CPK model: yellow, phosphorus; red, oxygen.) to the active site of ALP (presented as solid ribbons). (A) L-Peptide based precursor (**1a**) and (B) D-peptide based precursor (**1b**) binding to the phosphatase. (C) Top view and (D) side view of **1a** (green) and **1b** (dark pink) in the active site. Purple atoms represent the parts of **1a** and **1b** that would occupy the same space in the active site.

advantageous to develop a system that not only undergoes enzymatic hydrogelation but also forms hydrogels or nanofibers that are stable for a prolong period inside cells or in vivo. Among the strategies for improving stability of peptidic materials, the use of a D-amino acid to replace an L-amino acid is an effective one.²⁷ In addition to being protease resistant, D-peptides also are of considerable biological relevance.²⁸ For example, D-peptides can play a special role in defense mechanisms as “alien” agents from other organisms,²⁹ act as potent inhibitors to block HIV-1 entry,³⁰ inhibit tumor cell migration,³¹ reduce adverse drug reactions (ADRs),⁴ control the formation and disassembly of bacteria biofilms,³² bind to DNA,³³ form β sheets,³⁴ and dissociate Alzheimer’s amyloid to reduce the cytotoxicity induced by amyloid.³⁵

The merits of D-peptides encourage us to explore D-amino acid based supramolecular hydrogels, which would provide stable scaffolds for long-term drug release. Our previous works show that D-peptide based hydrogels are resistant to proteases while the corresponding L-amino acid derived molecules undergo proteolytic hydrolysis. Recently, we also have found that D-peptides are able to improve the selectivity of nonsteroid anti-inflammatory drugs (NSAIDs) and the D-peptide derivatives can serve as the substrate of an enzyme for hydrogelation catalyzed by alkaline phosphatase (ALP).⁴ However, it is unclear why and how the D-peptide derivatives serve as the substrates of phosphatases for hydrogelation and what other potential applications are. To address these unanswered questions, we synthesize the precursors of hydrogelators that are made of D-amino acid residues or L-amino acid residues and evaluate the formation of the nanofibers of the hydrogelators via enzymatic dephosphorylation of this pair of enantiomeric substrates. Our results from kinetic studies performed by ³¹P NMR and rheology indicate that the chirality of the precursors affects little on the enzymatic hydrogelation when the dephosphorylation occurs from the L- or D-tyrosine phosphate residues of the precursors. Moreover, the attachment of therapeutic agents or fluorophores to the side chain of the phosphorylated D-peptides results in new precursors, which confer biostable or biocompatible hydrogels/nanofibers that may find applications in intratumoral chemotherapy or intracellular imaging. This work, as the first study that confirms the enzymatic hydrogelation of D-peptides and L-peptides to occur at almost the same rate, illustrates a useful approach and

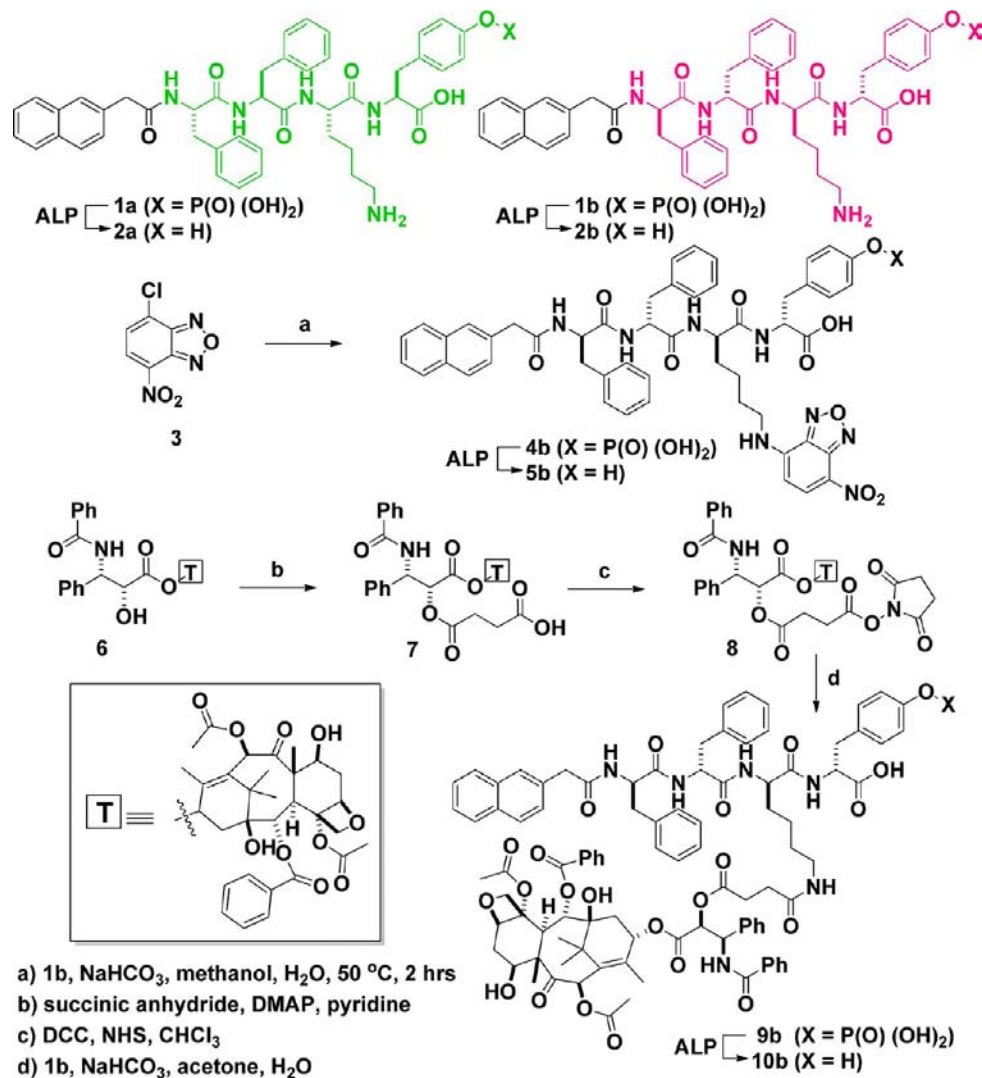
provides a new class of molecular platforms for generating supramolecular hydrogels that have both biostability and other desired functions for potential application inside cells or in vivo.

RESULTS AND DISCUSSION

Molecular Design. In our previous studies, we have found that the small dipeptide derivative 2-(naphthalen-2-yl)acetic-Phe-Phe (NapFF) is an excellent motif for enabling self-assembly and hydrogelation due to its strong supramolecular interactions arising from aromatic–aromatic interactions and hydrogen bonds among the molecules.³⁶ Since lysine (K) possesses an ϵ -amine site for the attachment of biofunctional molecules on the side chain and tyrosine phosphate (Y(p)) offers a handle for enzyme instructed hydrogelation, the incorporation of K and Y(p) with NapFF provides a versatile hydrogelator precursor NapFFKY(p) (**1a**), which undergoes enzymatic hydrogelation. Those studies suggest that one can use D-amino acids, D-Phe (f), D-Lys (k), and D-Tyr phosphate (y(p)), to replace the corresponding L-amino acids for making a more biostable precursor Napffky(p) (**1b**). To evaluate whether the dephosphorylation of D-tyrosine phosphate (y(p)) from the D-peptide by the phosphatase still would be possible, we first examine the binding of the tyrosine phosphate on **1a** or **1b** with ALP according to the crystal structure of ALP.³⁷ With the phosphate groups (represented by the yellow and red spheres in Figure 1) being anchored to the active site of ALP (represented by the solid ribbons in Figure 1), the structures of the phosphatase that binds with L-peptide/D-peptide based precursors **1a** and **1b** are shown in Figure 1A and B, respectively. Although there are stereochemical differences between **1a** and **1b**, the phosphate groups appear to be able to bind the same active site without any hindrance. According to the top view (Figure 1C), the opening in the structure of ALP is large enough to accommodate either **1a** or **1b**. Similarly, the side view (Figure 1D) clearly indicates that the phosphate groups on **1a** or **1b** are able to bind the active site of ALP. Thus, we choose to investigate the enzymatic hydrogelation of **1b** and to compare it with **1a** by the rate of formation, morphology, and viscoelastic property of the corresponding hydrogels.

To explore the biological and biomedical applications of **1b**, we attach small functional molecules, such as 4-nitro-2,1,3-benzoxadiazole (NBD), a fluorophore used in cell imaging, and

Scheme 1. Synthetic Route of the Precursor of the NBD- or Taxol-Containing Hydrogelator Based on a D-Peptide



taxol, a clinically used anticancer drug, to **1b**. Our previous works have established the synthetic route for the incorporation of the fluorophore or taxol to the hydrogelator precursor **1a**. For example, we have developed a fluorescent hydrogelator precursor that undergoes intracellular enzymatic hydrogelation and forms fluorescent molecular aggregates inside cells.³⁸ We have also attached taxol to **1a** to afford the precursor of an anticancer hydrogelator that increases the solubility of taxol and achieves controlled drug delivery.²² These studies offer the necessary synthetic routes that allow us to conjugate precursor **1b** with a NBD group or taxol, which affords Napffk(NBD)-y(p) (**4b**) or Napffk(taxol)y(p) (**9b**). These molecules represent a new type of precursors to result in the hydrogelators that are both biostable and multifunctional.

Synthesis. Scheme 1 shows the chemical structures of precursors **1a** and **1b**. Utilizing Fmoc-protected D-amino acids, we prepare **1b** by standard solid phase synthesis with 2-chlorotrityl chloride resin (100–200 mesh and 0.3–0.8 mmol/g), followed by high-performance liquid chromatography (HPLC) purification. We conjugate a NBD group at the side chain of lysine to afford the precursor Napffk(NBD)y(p) (**4b**). As shown in Scheme 1, we dissolve 7-chloro-4-nitro-2,1,3-benzoxadiazole (NBD-Cl) (**3**) in methanol, followed by adding the basic aqueous solution of **1b** (pH 9). The reaction of the

mixed solution at 50 °C for 2 h yields **4b** as orange-red precipitates after workup and purification by reverse-phase HPLC.

Using a similar approach, we obtain the conjugate of taxol and **1b**. As shown in Scheme 1, we add succinic anhydride and 4-dimethylamino-pyridine (DMAP) into the clear solution of taxol (**10**) in pyridine. After stirring the mixture at room temperature overnight, we extract the solution with dichloromethane (DCM) and obtain taxol-succinic acid (**7**). The conjugation of **7** and *N*-hydroxysuccinimide (NHS) with the aid of *N,N'*-dicyclohexylcarbodiimide (DCC) affords taxol-succinic-NHS ester (**8**). Using column chromatography for purification, we collect pure **8** and redissolve it with acetone. Then, we add the acetone solution into a basic aqueous solution (pH 8.5) of **5b**, which reacts for 24 h. After working up the reaction and using reverse-phase HPLC for the purification, we obtain compound **9b** as the conjugate of taxol and **1b**. These results indicate that it is convenient to apply the synthesis of L-peptidic precursors for producing the corresponding D-peptidic precursors.

Hydrogelation of the D-Peptidic Hydrogelator (2b). To investigate the enzymatic hydrogelation of the D-peptidic precursor **1b**, we prepare a series of hydrogels formed by using ALP to treat **1b** at different concentrations. After

dissolving 1.0, 2.0, 3.0, 4.0, and 5.0 mg of **1b** in 0.5 mL of water (pH 7.6), respectively, we obtain clear solutions of **1b** with different concentrations. The treatment of the solutions of **1b** with ALP (1.0 U/mL) affords the molecules of hydrogelator **2b**, which are less soluble than **1b** and thus self-assemble in water to form hydrogels when the concentrations of **2b** are sufficient. As shown in Figure 2, except the solution of 0.2 wt %

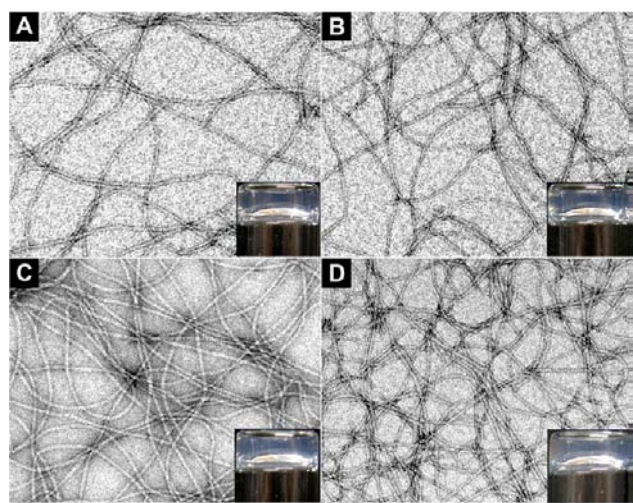


Figure 2. TEM images of the hydrogels formed by using ALP (1.0 U/mL) to treat **1b** at pH 7.6 and concentrations of (A) 0.4 wt %, (B) 0.6 wt %, (C) 0.8 wt %, and (D) 1.0 wt %. Inset: optical images. Scale bar is 100 nm.

of **1b**, solutions of **1b** with the concentrations of 0.4, 0.6, 0.8, or 1.0 wt % form a stable transparent hydrogel within 24 h after the addition of 1.0 U/mL ALP into the solutions. Furthermore, as shown in the optical images in Figure 2, the higher concentration of the solutions of **1b** gives the less transparent hydrogels of **2b**, which also exhibits little birefringence (Figure S6, Supporting Information), indicating that excess overlapping of the nanofibers to form large domains in the hydrogels of **2b** cause the scattering of the light.

Being complementary to the optical images that serve as a simple way for proving the macroscopic phase transition (i.e., hydrogelation) triggered by the addition of ALP, transmission electron microscopy (TEM) images reveal the ordered nanostructures (e.g., nanofibers), formed by the self-assembly of the hydrogelators, that lead to hydrogelation. As shown in Figure 2, the TEM images of all the hydrogels, which consist of different concentrations of **2b**, exhibit long, flexible, and uniform nanofibers that entangle to form stable networks. With the increase of the concentrations of hydrogelator **2b** (0.4, 0.6, 0.8, and 1.0 wt %), the densities of the nanofibers in the hydrogels increase, but the widths of the nanofibers in the hydrogels remain similar (around 9 ± 2 nm). These results indicate that the concentration of the hydrogelator **2b** hardly affects the self-assembling process controlled by the enzymatic hydrogelation so that the nanofibers exhibit similar morphology regardless of the concentrations of the precursor solutions. The concentrations of the hydrogelators correlate well with the densities of nanofibers, which should match with the viscoelastic behaviors of the hydrogels.

The oscillatory rheological measurement of the hydrogels of **2b** agrees with the density of the nanofibers in the hydrogels. The dynamic strain sweep, under constant oscillation

frequencies and various oscillation strains, indicates that the storage moduli (G') of all these hydrogels are independent to strain until their critical strains reach and G' values start to decrease drastically due to the breakdown of the networks of the hydrogels. After obtaining the maximum G' values of the hydrogels in dynamic strain sweep, we measure the frequency dependence of their storage moduli (G') and loss moduli (G'') using dynamic frequency sweep at constant oscillation strain (the strain for maximum G' values) and temperature (25 °C) but varying oscillation frequency (0.1–200 rad/s). All the hydrogels of **2b** exhibit viscoelastic properties of solidlike materials, evidenced by the fact that their G' values are significantly higher (more than five times) than those of their G'' values and are independent of the frequency during dynamic frequency sweep (Figure S8, Supporting Information). As listed in Table 1, the hydrogels of **2b** at the concentrations

Table 1. Rheological Properties and TEM Characteristics of the Hydrogels of **2a**, **2b**, **5b**, and **10b**

compd	conc (wt %)	dynamic strain sweep		dynamic frequency sweep	
		maximum G' (Pa)	critical strain (%)	G'^a (Pa)	width of fiber (nm)
2a	0.4	7.2×10^2	3.7	8.6×10^2	8 ± 2
2b	0.4	6.4×10^2	4.7	6.5×10^2	8 ± 2
	0.6	1.7×10^3	5.0	1.8×10^3	9 ± 2
	0.8	2.7×10^3	14	2.7×10^3	9 ± 2
	1.0	3.9×10^3	16	3.8×10^3	9 ± 2
5b^b	0.4	46	6.9	62	8 ± 2
10b^b	1.8	43	0.59	16	9 ± 2

^aThe value is taken at a frequency equal to 6.28 rad/s. ^bThe hydrogel is formed at pH 7.4, while others are formed at pH 7.6.

of 0.4, 0.6, 0.8, and 1.0 wt % exhibit strains of 4.7%, 5.0%, 14%, and 16%, respectively. In addition, their G' values (at the frequency of 6.28 rad/s) in dynamic frequency sweep are 6.5×10^2 , 1.8×10^3 , 2.7×10^3 , and 3.8×10^3 Pa. While the critical strains of the resulting hydrogels of **2b** show little correlation with the concentrations of the hydrogelators (Figures S8C and S8D, Supporting Information), the storage moduli of hydrogels of **2b** increase with the concentrations of **2b**. This result agrees with more physical cross-linking of the nanofibers at high concentrations of the hydrogelators.

Comparisons of L- and D-Enantiomers of the Precursors and Hydrogelators. The comparison of the enzymatic hydrogelation processes of **1a** and **1b** under the same conditions reveals that the chirality of **1a** and **1b** affects little on their dephosphorylation and the subsequent hydrogelation. To evaluate the rate of the enzymatic hydrogelation process, we use ³¹P NMR and rheology to study the transformation of the precursors **1a** and **1b** upon the treatment of ALP (Figure 3). We first dissolve 10 mg of **1a** and **1b** into 1.0 mL of water at pH 7.6, respectively, to afford clear solutions with concentrations of 1.0 wt %. Once adding 0.02 U/mL of alkaline phosphates, we immediately monitor the solutions of **1a** and **1b** by ³¹P NMR and oscillatory rheology at 25 °C. The ³¹P NMR spectra at 3 min, 4, 12, 24, and 48 h indicate that the phosphate groups on the L-tyrosine of **1a** and D-tyrosine **1b** ($\delta = -2.7$) become free phosphates ($\delta = 0.0$) at almost the same rate and dephosphorylation finishes after 48 h. This result suggests that the precursors **1a** and **1b** undergo dephosphor-

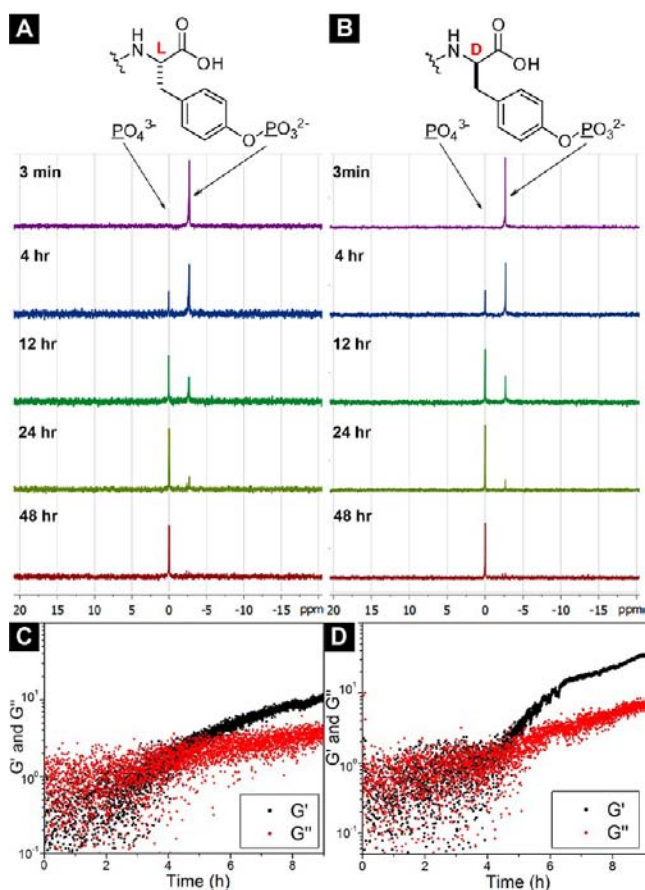


Figure 3. ^{31}P NMR shows the conversion of 1.0 wt % of (A) **1a** and (B) **1b** catalyzed by the phosphatase (0.02 U/mL) at pH 7.6 at 3 min and 4, 12, 24, and 48 h. Time-dependent rheology study of 1.0 wt % of (C) **1a** and (D) **1b** catalyzed by the phosphatase (0.02 U/mL) at pH 7.6.

ylation at similar rates upon being treated with ALP. Figure 3C,D displays the time-dependent rheology studies of **1a** and **1b**. At the beginning, values of G'' are higher than the values of G' for the solutions of **1a** and **1b**, indicating both of them are fluids. However, as **1a** and **1b** slowly turn into hydrogelators **2a** and **2b**, respectively, by enzymatic dephosphorylation, the solutions start to form solidlike hydrogels with values of G' becoming higher than those of G'' . The gelation points for **2a** and **2b**, at where G' values intersect with G'' values, are both achieved around 5 h after the addition of enzyme. This result, together with the ^{31}P NMR experiment, suggests that the chirality of **1a** and **1b** exhibits almost the same influence on the enzymatic hydrogelation catalyzed by ALP. The oscillatory shear during the rheological measurement may accelerate enzymatic dephosphorylation so that the gelation points reach at the time (5 h) much shorter than the time for complete dephosphorylation during the NMR experiment (48 h).

After comparing the rate of the dephosphorylation of the L- and D-enantiomeric precursors (**1a** and **1b**), we examine the morphology of the microstructures and viscoelastic properties of the corresponding hydrogels (**2a** and **2b**). By sonication, we dissolve 2.0 mg of **1a** or **1b** into 0.5 mL of water at pH 7.6 to afford a clear solution. The addition of 1.0 U/mL of ALP into the solution of **1a** or **1b** turns the hydrogelator precursor to its corresponding hydrogelator, **2a** or **2b**, which results in a transparent hydrogel (0.4 wt %) within 24 h. As shown in

Figure 4A,B, both hydrogelators **2a** and **2b** self-assemble to form long, flexible, and uniform nanofibers with average widths

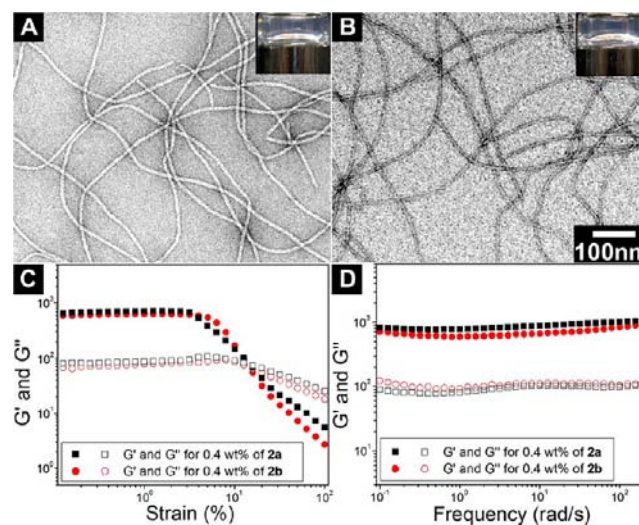


Figure 4. Optical images and TEM images of the hydrogels formed by using ALP (1.0 U/mL) to treat 0.4 wt % of (A) **1a** and (B) **1b** at pH 7.6. (C) Strain sweep and (D) frequency sweep of the hydrogels **2a** and **2b**.

around 8 ± 2 nm, which entangle to develop physically cross-linked networks and to afford stable hydrogels. The similarity of the nanofibers in these two hydrogels indicates that chirality of **2a** and **2b** has similar influence on the morphology of their nanofibers. Oscillatory rheology of the hydrogels of **2a** and **2b** indicates that both hydrogels behave as solidlike materials that have storage moduli (G') that are significantly higher than loss moduli (G'') and exhibit weak frequency dependence in dynamic frequency sweep (Figure 4C,D). As shown in Table 1, hydrogels of **2a** and **2b** have critical strains of 3.7% and 4.7% during the dynamic strain sweep, and their values of G' (at the frequency of 6.28 rad/s) in dynamic frequency sweep are 8.6×10^2 and 6.5×10^2 Pa, respectively. These results suggest that the chirality of these two hydrogelators causes negligible differences on the viscoelastic properties of the corresponding hydrogels.

Application of the D-Enantiomer Hydrogelator (1b) for Potential Intracellular Imaging. According to the molecular design, the attachment of functional molecules to **1b** broadens the scope of the applications of supramolecular hydrogelators in cells or in vivo. We first examine the feasibility and characteristic of the use of **4b** for imaging intracellular self-assembly of D-peptidic hydrogelators. After dissolving 2.0 mg of **4b** into 0.5 mL of water at pH 7.4, we treat the clear orange solution with 20.0 U/mL ALP, which turns **4b** into the fluorescent hydrogelator **5b**. The self-assembly of **5b** affords a transparent orange hydrogel (Figure 5A, inset) that is stable over weeks. The TEM image of the hydrogel of **5b** exhibits long and uniform nanofibers with average widths of 8 ± 2 nm that entangle to afford a stable network (Figure 5A). According to our previous study, the unassociated molecules of NBD-containing hydrogelators in aqueous solutions exhibit little fluorescence unless they aggregate to form nanofibers.³⁸ This important feature makes a NBD-containing hydrogelator a useful candidate for imaging molecular self-assembly inside cells.

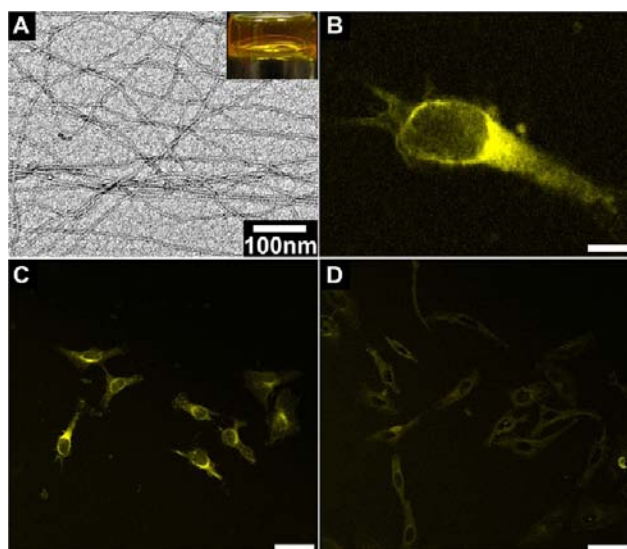


Figure 5. (A) Optical image and TEM image of hydrogel formed by 0.4 wt % of **4b** at pH 7.4 upon the catalysis of ALP (20.0 U/ml). (B) Fluorescent confocal microscope image of a HeLa cell incubated with 500 μM **4b** in phosphate-buffered saline (scale bar is 10 μm). (C) Fluorescent confocal microscope images of HeLa cells incubated with 500 μM **4b** without (C) or with (D) the PTP1B inhibitor (25 μM) (scale bar is 50 μm).

After treating HeLa cells with 500 μM hydrogelator precursor **4b** for 2 min, we observe strong fluorescence emerging from the region near the nuclei of the cells (Figure 5B, C), suggesting that the self-assembly of **5b** results in formation of the nanofibers of **5b** around the endoplasmic reticulum (ER). There is little fluorescence outside the cells, suggesting the lack of dephosphorylation and/or self-assembly of **5b**. To confirm that the dephosphorylation of **4b** and self-assembly of **5b** take place in the ER, we use 25 μM CinnGEL 2Me to inhibit protein tyrosine phosphatase-1B (PTP1B),³⁹ a highly efficient phosphatase located at the outer membrane of the ER, when the HeLa cells are incubated with **4b** (500 μM). As shown in Figure 5D, the addition of the inhibitor of PTP1B significantly decreases and delays the fluorescence inside the cells, confirming that the dephosphorylation of **4b** and the self-assembly of **5b** occur at the ER. As shown by the time sequence fluorescent images of the HeLa cells incubated with **4b** in the absence of the PTP1B inhibitor (Figure S11, Supporting Information), most of the cells exhibit strong fluorescence after being treated with **4b** for only 2 min. Even being incubated with the presence of the PTP1B inhibitor, the cells still show partial fluorescence after 5 min of the incubation. Apparently, the fluorescence of the nanofibers in the HeLa cells treated by the D-peptide precursor (**4b**) emerges much faster than that of L-peptide precursor (**4a**) (which takes about 15 min³⁸ in the presence of CinnGEL 2Me). This result agrees with the fact that the resulted D-peptide hydrogelator (**5b**) is more resistant to proteolytic degradation than the L-peptide hydrogelator (**5a**) is.

Application of D-Enantiomer Hydrogelator (1b) for Potential Intratumoral Chemotherapy. Typically, after dissolving 9.0 mg of **9b** in 0.5 mL of water at pH 7.4 by sonication, we add ALP (1.0 U/mL) into the solution of **9b** to obtain hydrogelator **10b**, which forms a stable and semi-transparent hydrogel (Figure 6A). This result differs slightly from the behavior of precursor **9a** that undergoes enzymatic

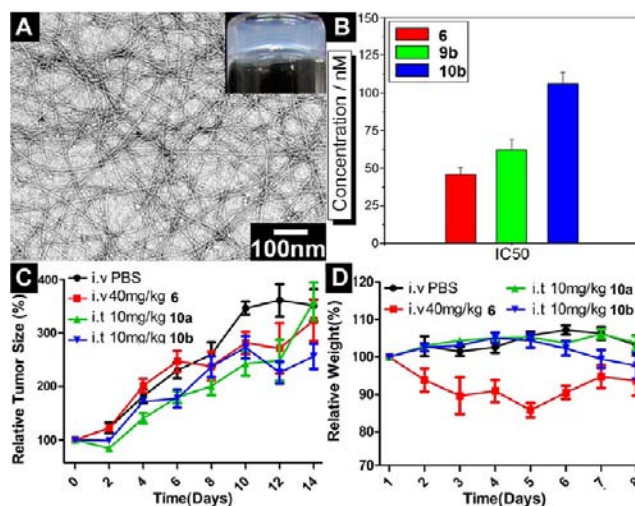


Figure 6. (A) Optical and TEM images of hydrogel formed by 1.8 wt % of **10b** at pH 7.4 with the catalysis of ALP (1 U/mL) with a scale of 100 nm. (B) IC_{50} values of **6**, **9b**, and **10b** incubated with HeLa cells after 72 h. (C) Relative tumor sizes and (D) relative weights of mice treated with **6**, **10a**, and **10b** for in vivo tests.

hydrogelation at the concentration of 1.0 wt %, ²² suggesting that precursor **9b** (having a concentration up to 1.8 wt % for enzymatic hydrogelation) and hydrogelator **10b** exhibit relatively good solubility. This subtle increase of the solubility should increase the amount of taxol in the hydrogel. The TEM image of hydrogel **10b** shows uniform nanofibers with average widths of 9 ± 2 nm. To determine the efficacies of taxol after conjugating it into the hydrogelator, we use MTT assays to examine the viability of HeLa cells incubated with taxol (**6**), **9b**, and **10b** for 72 h at 37 $^{\circ}\text{C}$. Figure 6B shows the IC_{50} values of **6**, **9b**, and **10b**, which are 45.8, 61.9, and 105.9 nM, respectively. This result suggests that the conjugation of taxol to the D-peptide essentially preserves the antitumor activity of taxol, thus encouraging us to carry out an in vivo test of **10b** on a mouse model.⁴⁰

As expected, both L- and D-peptide based hydrogels of **10a** and **10b** exhibit similar antitumor activities up to 12 days of intratumoral injection of the hydrogels. After inoculating female Balb/c mice with 2×10^5 of 4T1-luciferase cells in the mammary fat pad, we allow tumors to grow until their sizes reach about 500 mm^3 , and we randomly divide them into different treatment groups: (1) intravenous injections of phosphate-buffered saline (PBS) vehicle control; (2) intravenous injection of 4×10 mg/kg of taxol every other day from day 0 for indicated times; (3) a single intratumoral injection of 10 mg/kg of taxol containing hydrogels in 40 μL volume. With the treatments of **6** (taxol), **10a**, **10b**, or PBS buffer (control) for 14 days, we monitor the relative tumor sizes (calculated by the following formula: tumor volume = length \times width \times (length + width)/2) and relative weights of mice every 2 days. Due to the toxicity of clinical taxol (formulated with Cremophor EL),⁴¹ the single injection of 40 mg/kg of taxol may cause death of the mouse immediately. Therefore, we have to divide 40 mg/kg of **6** into four injections with each injection of 10 mg/kg. As shown in Figure 6C, the intravenous injections of 40 mg/kg of **6** every other day from day 0 results in the relative tumor sizes to be smaller than those of the control group after day 8. In contrast, the intratumoral injections of the hydrogels **10a** or **10b** at only one dose of 10 mg/kg in the mice

at day 0, which may sustain for 1 month, reduce the relative tumor sizes on the mice more significantly than those of the controls after day 2. At day 14, although the relative tumor sizes in the groups injected with **6** and the hydrogel of **10a** are similar with the PBS control group, the relative tumor size in the group injected with the hydrogel of **10b** is statistically smaller than the control. This result suggests that the hydrogel of **10b** exhibits higher antitumor efficacy than **10a** or **6** do. Figure 6D shows the relative weights of mice during these 14 days treatment, suggesting that the intratumoral injection of hydrogels of **10a** and **10b** only once certainly limit the side effect of taxol to the mice. These results support that the local injection of the hydrogels appears to achieve long-term drug release with higher efficacy and better biocompatibility than the intravenous injection of taxol.⁴⁰ This promising result warrants further investigation of the D-peptidic hydrogels of taxol on animal models.

CONCLUSION

In conclusion, taking the advantages of D-amino acids, we have developed biostable and biocompatible supramolecular hydrogels made of D-amino acid residues. Similar to other D-amino acid containing peptides, **1b** resists proteases while the corresponding L-amino acid derived molecule (**1a**) undergoes proteolytic hydrolysis (Figure S12, Supporting Information). Although these D-peptidic derivatives are intrinsically resistant to proteolytic hydrolysis, which make the hydrogels stable platform materials for long-term biomedical applications, the D-peptide based hydrogelator precursor still acts as a substrate of phosphatase for enzyme-instructed self-assembly. While it appears unexpected that the rates of dephosphorylation of L- and D-peptide precursors are comparable, the crystal structure of the phosphatase confirms it is feasible for such an observation. This work thus illustrates a protein structure-based approach for designing the substrates of enzyme-instructed self-assembly and hydrogelation. While the conjugation of **1b** with taxol affords a biostable hydrogel that exhibits improved drug efficacy in anticancer activity, the fast accumulation of molecular nanofibers of D-peptide (in the case of **4b**) is particularly intriguing because it indicates the introduction of D-peptide may result in certain biological effects much faster than intuitively thought, which is a subject worthwhile for the further exploration.

ASSOCIATED CONTENT

Supporting Information

Details of the synthesis, NMR spectra, and LC-MS data for all compounds, rheological data, cytotoxicity data, and in vivo tests. This material is available free of charge via the Internet at <http://pubs.acs.org>.

AUTHOR INFORMATION

Corresponding Author

bxu@brandeis.edu

Notes

The authors declare no competing financial interest.

ACKNOWLEDGMENTS

This work was partially supported by HFSP (RGP0056/2008), a start-up fund from Brandeis University, and NIH (R01CA142746). The TEM images were taken at the Brandeis EM and Optical Imaging facilities.

REFERENCES

- (1) (a) Terech, P.; Weiss, R. G. *Chem. Rev.* **1997**, *97*, 3133–3159. (b) Heeres, A.; van der Pol, C.; Stuart, M. C. A.; Friggeri, A.; Feringa, B. L.; van Esch, J. *J. Am. Chem. Soc.* **2003**, *125*, 14252–14253. (c) Mukhopadhyay, S.; Maitra, U.; Ira; Krishnamoorthy, G.; Schmidt, J.; Talmon, Y. *J. Am. Chem. Soc.* **2004**, *126*, 15905–15914. (d) Zhang, Y.; Yang, Z. M.; Yuan, F.; Gu, H. W.; Gao, P.; Xu, B. *J. Am. Chem. Soc.* **2004**, *126*, 15028–15029. (e) Vemula, P. K.; Li, J.; John, G. *J. Am. Chem. Soc.* **2006**, *128*, 8932–8938. (f) Yang, Z. M.; Liang, G. L.; Wang, L.; Xu, B. *J. Am. Chem. Soc.* **2006**, *128*, 3038–3043. (g) Cai, W.; Wang, G. T.; Du, P.; Wang, R. X.; Jiang, X. K.; Li, Z. T. *J. Am. Chem. Soc.* **2008**, *130*, 13450–13459. (h) Ma, M. L.; Kuang, Y.; Gao, Y.; Zhang, Y.; Gao, P.; Xu, B. *J. Am. Chem. Soc.* **2010**, *132*, 2719–2728. (i) Li, X. M.; Kuang, Y.; Shi, J. F.; Gao, Y.; Lin, H. C.; Xu, B. *J. Am. Chem. Soc.* **2011**, *133*, 17513–17518. (j) Zheng, W. T.; Gao, J.; Song, L. J.; Chen, C. Y.; Guan, D.; Wang, Z. H.; Li, Z. B.; Kong, D. L.; Yang, Z. M. *J. Am. Chem. Soc.* **2013**, *135*, 266–271. (k) Xing, B. G.; Yu, C. W.; Chow, K. H.; Ho, P. L.; Fu, D. G.; Xu, B. *J. Am. Chem. Soc.* **2002**, *124*, 14846–14847.
- (2) Estroff, L. A.; Hamilton, A. D. *Chem. Rev.* **2004**, *104*, 1201–1217.
- (3) (a) Komatsu, H.; Matsumoto, S.; Tamaru, S.; Kaneko, K.; Ikeda, M.; Hamachi, I. *J. Am. Chem. Soc.* **2009**, *131*, 5580–5585. (b) Boekhoven, J.; Koot, M.; Wezendonk, T. A.; Eelkema, R.; van Esch, J. H. *J. Am. Chem. Soc.* **2012**, *134*, 12908–12911.
- (4) Li, J. Y.; Kuang, Y.; Gao, Y.; Du, X. W.; Shi, J. F.; Xu, B. *J. Am. Chem. Soc.* **2013**, *135*, 542–545.
- (5) (a) Hartgerink, J. D.; Beniash, E.; Stupp, S. I. *Science* **2001**, *294*, 1684–1688. (b) Holmes, T. C.; de Lacalle, S.; Su, X.; Liu, G. S.; Rich, A.; Zhang, S. G. *Proc. Natl. Acad. Sci. U.S.A.* **2000**, *97*, 6728–6733. (c) Haines, L. A.; Rajagopal, K.; Ozbas, B.; Salick, D. A.; Pochan, D. J.; Schneider, J. P. *J. Am. Chem. Soc.* **2005**, *127*, 17025–17029. (d) Galler, K. M.; Aulisa, L.; Regan, K. R.; D'Souza, R. N.; Hartgerink, J. D. *J. Am. Chem. Soc.* **2010**, *132*, 3217–3223.
- (6) Zhao, F.; Ma, M. L.; Xu, B. *Chem. Soc. Rev.* **2009**, *38*, 883–891.
- (7) (a) Wada, A.; Tamaru, S.; Ikeda, M.; Hamachi, I. *J. Am. Chem. Soc.* **2009**, *131*, 5321–5330. (b) Rajagopalan, A.; Kroutil, W. *Mater. Today* **2011**, *14*, 144–152.
- (8) Bremmer, S. C.; Chen, J.; McNeil, A. J.; Soellner, M. B. *Chem. Commun.* **2012**, *48*, 5482–5484.
- (9) Yang, Z. M.; Liang, G. L.; Ma, M. L.; Abbah, A. S.; Lu, W. W.; Xu, B. *Chem. Commun.* **2007**, 843–845.
- (10) Kiyonaka, S.; Sada, K.; Yoshimura, I.; Shinkai, S.; Kato, N.; Hamachi, I. *Nat. Mater.* **2004**, *3*, 58–64.
- (11) Yamamichi, S.; Jinno, Y.; Haraya, N.; Oyoshi, T.; Tomitori, H.; Kashiwagi, K.; Yamanaka, M. *Chem. Commun.* **2011**, *47*, 10344–10346.
- (12) Yang, Z. M.; Kuang, Y.; Li, X. M.; Zhou, N.; Zhang, Y.; Xu, B. *Chem. Commun.* **2012**, *48*, 9257–9259.
- (13) Gao, Y.; Long, M. J. C.; Shi, J. F.; Hedstrom, L.; Xu, B. *Chem. Commun.* **2012**, *48*, 8404–8406.
- (14) (a) Cui, H. G.; Webber, M. J.; Stupp, S. I. *Biopolymers* **2010**, *94*, 1–18. (b) Williams, R. J.; Mart, R. J.; Ulijn, R. V. *Biopolymers* **2010**, *94*, 107–117. (c) Rajagopal, K.; Ozbas, B.; Pochan, D. J.; Schneider, J. P. *Biopolymers* **2005**, *80*, 487–487. (d) Gao, Y.; Yang, Z. M.; Kuang, Y.; Ma, M. L.; Li, J. Y.; Zhao, F.; Xu, B. *Biopolymers* **2010**, *94*, 19–31.
- (15) Chan, W. C.; White, P. *Fmoc Solid Phase Peptide Synthesis: A Practical Approach*; Oxford University Press: Oxford, U.K., 2000.
- (16) Hu, B. H.; Messersmith, P. B. *J. Am. Chem. Soc.* **2003**, *125*, 14298–14299.
- (17) (a) Yang, Z. M.; Gu, H. W.; Fu, D. G.; Gao, P.; Lam, J. K.; Xu, B. *Adv. Mater.* **2004**, *16*, 1440–1444. (b) Toledano, S.; Williams, R. J.; Jayawarna, V.; Ulijn, R. V. *J. Am. Chem. Soc.* **2006**, *128*, 1070–1071. (c) Yang, Z.; Liang, G.; Xu, B. *Acc. Chem. Res.* **2008**, *41*, 315–326. (d) Hirst, A. R.; Roy, S.; Arora, M.; Das, A. K.; Hodson, N.; Murray, P.; Marshall, S.; Javid, N.; Sefcik, J.; Boekhoven, J.; van Esch, J. H.; Santabarbara, S.; Hunt, N. T.; Ulijn, R. V. *Nat. Chem.* **2010**, *2*, 1089–1094. (e) Williams, R. J.; Smith, A. M.; Collins, R.; Hodson, N.; Das, A. K.; Ulijn, R. V. *Nat. Nanotechnol.* **2009**, *4*, 19–24.
- (18) Yang, Z. M.; Xu, B. *Chem. Commun.* **2004**, 2424–2425.

- (19) Schnepf, Z. A. C.; Gonzalez-McQuire, R.; Mann, S. *Adv. Mater.* **2006**, *18*, 1869–1872.
- (20) Yang, Z. M.; Ho, P. L.; Liang, G. L.; Chow, K. H.; Wang, Q. G.; Cao, Y.; Guo, Z. H.; Xu, B. *J. Am. Chem. Soc.* **2007**, *129*, 266–267.
- (21) (a) Vemula, P. K.; Cruikshank, G. A.; Karp, J. M.; John, G. *Biomaterials* **2009**, *30*, 383–393. (b) Williams, R. J.; Hall, T. E.; Glattauer, V.; White, J.; Pasic, P. J.; Sorensen, A. B.; Waddington, L.; McLean, K. M.; Currie, P. D.; Hartley, P. G. *Biomaterials* **2011**, *32*, 5304–5310.
- (22) Gao, Y.; Kuang, Y.; Guo, Z. F.; Guo, Z. H.; Krauss, I. J.; Xu, B. *J. Am. Chem. Soc.* **2009**, *131*, 13576–+.
- (23) Wang, Q. G.; Yang, Z. M.; Gao, Y.; Ge, W. W.; Wang, L.; Xu, B. *Soft Matter* **2008**, *4*, 550–553.
- (24) (a) Yang, Z. M.; Xu, K. M.; Guo, Z. F.; Guo, Z. H.; Xu, B. *Adv. Mater.* **2007**, *19*, 3152–3156. (b) Yang, Z.; Liang, G.; Guo, Z.; Xu, B. *Angew. Chem., Intl. Ed.* **2007**, *46*, 8216–8219.
- (25) Cheetham, A. G.; Zhang, P. C.; Lin, Y. A.; Lock, L. L.; Cui, H. *G. J. Am. Chem. Soc.* **2013**, *135*, 2907–2910.
- (26) Gao, Y.; Shi, J. F.; Yuan, D.; Xu, B. *Nat. Commun.* **2012**, *3*, 1033.
- (27) (a) Li, X. M.; Du, X. W.; Li, J. Y.; Gao, Y.; Pan, Y.; Shi, J. F.; Zhou, N.; Xu, B. *Langmuir* **2012**, *28*, 13512–13517. (b) Liang, G. L.; Yang, Z. M.; Zhang, R. J.; Li, L. H.; Fan, Y. J.; Kuang, Y.; Gao, Y.; Wang, T.; Lu, W. W.; Xu, B. *Langmuir* **2009**, *25*, 8419–8422.
- (28) (a) Van Regenmortel, M. H. V.; Muller, S. *Curr. Opin. Biotechnol.* **1998**, *9*, 377–382. (b) Nair, D. T.; Kaur, K. J.; Singh, K.; Mukherjee, P.; Rajagopal, D.; George, A.; Bal, V.; Rath, S.; Rao, K. V. S.; Salunke, D. M. *J. Immunol.* **2003**, *170*, 1362–1373.
- (29) Konno, R. *D-amino Acids: A New Frontier in Amino Acids and Protein Research: Practical Methods and Protocols*; Nova Science Publishers: Hauppauge, NY, 2007; Vol. 35.
- (30) Welch, B. D.; VanDemark, A. P.; Heroux, A.; Hill, C. P.; Kay, M. *S. Proc. Natl. Acad. Sci. U.S.A.* **2007**, *104*, 16828–16833.
- (31) (a) Sroka, T. C.; Pennington, M. E.; Cress, A. E. *Carcinogenesis* **2006**, *27*, 1748–1757. (b) Liu, M.; Li, C.; Pazgier, M.; Li, C. Q.; Mao, Y. B.; Lv, Y. F.; Gu, B.; Wei, G.; Yuan, W. R.; Zhan, C. Y.; Lu, W. Y. *Proc. Natl. Acad. Sci. U.S.A.* **2010**, *107*, 14321–14326.
- (32) Kolodkin-Gal, I.; Romero, D.; Cao, S. G.; Clardy, J.; Kolter, R.; Losick, R. *Science* **2010**, *328*, 627–629.
- (33) (a) Reich, Z.; Schramm, O.; Brumfeld, V.; Minsky, A. *J. Am. Chem. Soc.* **1996**, *118*, 6345–6349. (b) Morii, T.; Tanaka, T.; Sato, S.; Hagihara, M.; Aizawa, Y.; Makino, K. *J. Am. Chem. Soc.* **2002**, *124*, 180–181. (c) Michaud, M.; Jourdan, E.; Villet, A.; Ravel, A.; Grosset, C.; Peyrin, E. *J. Am. Chem. Soc.* **2003**, *125*, 8672–8679.
- (34) Swanekamp, R. J.; DiMaio, J. T. M.; Bowerman, C. J.; Nilsson, B. L. *J. Am. Chem. Soc.* **2012**, *134*, 5556–5559.
- (35) (a) Esteras-Chopo, A.; Pastor, M. T.; Serrano, L.; de la Paz, M. L. *J. Mol. Biol.* **2008**, *377*, 1372–1381. (b) Chalifour, R. J.; McLaughlin, R. W.; Lavoie, L.; Morissette, C.; Tremblay, N.; Boule, M.; Sarazin, P.; Stea, D.; Lacombe, D.; Tremblay, P.; Gervais, F. *J. Biol. Chem.* **2003**, *278*, 34874–34881.
- (36) (a) Lehn, J. M. *Angew. Chem., Intl. Ed. Engl.* **1988**, *27*, 89–112. (b) Whitesides, G. M.; Grzybowski, B. *Science* **2002**, *295*, 2418–2421.
- (37) Coleman, J. E. *Annu. Rev. Biophys. Biomol. Struct.* **1992**, *21*, 441–483.
- (38) Gao, Y.; Shi, J. F.; Yuan, D.; Xu, B. *Nat. Commun.* **2012**, *3*, 1033.
- (39) Frangioni, J. V.; Beahm, P. H.; Shifrin, V.; Jost, C. A.; Neel, B. G. *Cell* **1992**, *68*, 545–560.
- (40) Wang, H. M.; Wei, J.; Yang, C. B.; Zhao, H. Y.; Li, D. X.; Yin, Z. N.; Yang, Z. M. *Biomaterials* **2012**, *33*, 5848–5853.
- (41) Rowinsky, E. K.; Eisenhauer, E. A.; Chaudhry, V.; Arbut, S. G.; Donehower, R. C. *Semin. Oncol.* **1993**, *20*, 1–15.